# Characterizations of flax fabric reinforced nanoclay-geopolymer composites

H. Assaedi[1,2], F.U.A. Shaikh[3], I.M. Low[1,*]

[1)] Department of Imaging & Applied Physics, Curtin University, GPO Box U1987, Perth, WA 6845, Australia

[2)] Department of Physics, Umm Al-Qura University, P.O. Box 715, Makkah, Saudi Arabia.

[3)] Department of Civil Engineering, Curtin University, GPO Box U1987, Perth, WA 6845, Australia

*Corresponding author. j.low@curtin.edu.au; Tel.: +61 8 9266 7544; fax: +61 8 9266 2377.

## Abstract

Geopolymer composites reinforced with flax fabrics (FF) and nanoclay platelets are synthesised and studied in terms of physical and mechanical properties. X-Ray Diffraction (XRD), Fourier transform infrared spectroscopy (FTIR), Scanning Electron Microscope (SEM) techniques are used for phase and microstructure characterisation. The nanoclay platelets are added to reinforce the geopolymer matrices at 1.0%, 2.0%, and 3.0% by weight. It is found that 2.0 wt.% nanoclay enhances the density, decreases the porosity and subsequently improves the flexural strength and toughness. The microstructural analysis results indicate that the nanoclay behaves not only as a filler to improve the microstructure of the binder, but also as an activator to support the geopolymeric reaction producing higher content of geopolymer gel. This enhances the adhesion

between geopolymer matrix and flax fibres, which improves the mechanical properties of the geopolymer nanocomposites reinforced with flax fabrics.

**Keywords**

Geopolymer; flax fibre; nanoclay; physical properties; mechanical properties.

## Introduction

Ordinary Portland cements are widely used in construction applications due to their suitable mechanical and durability properties. Greenhouse emissions from the production of such cement-based materials, however, have necessitated the search for eco-friendly alternatives. Geopolymer is one such alternative. This material, first introduced by Davidovits (1989), exhibit durability, good mechanical performance and fire and acid resistance. The production of geopolymers, being cured at room temperature is considerably more ecologically friendly than the production of Portland cement. It is a process that offers 80-90% reduction in carbon dioxide emission [1-5].

Despite promising characteristics of geopolymers, the material's matrix is one which suffers brittle failure readily under applied force and typically demonstrates poor flexural strength [6, 7]. Improving the mechanical properties such as flexural strength and toughness of geopolymers will significantly increase its application in the construction and building industries; and this may be accomplished by two ways [8]: one is to develop ‘environmental-friendly materials’ through utilizing natural fibres as fibre-reinforced geopolymer composite, and the other is to improve the physical properties of the matrix by adding nanoparticles to the geopolymer paste.

The advantages of using natural fibres in composites include the low density, flexibility and the high modulus [9, 10]. Other advantages in addition to good mechanical properties include biodegradable, renewable and recyclable nature of natural fibres [11]. These characteristics have made natural fibres attractive to be utilized as reinforcement in various composites systems. For instance, cellulose extracted from wood materials is used to strengthen polymers and epoxy [12, 13]. Bamboo and wood fibres are also used in the strengthening of concrete and known for the flexural advantages [14, 15]. Cotton fibres are used to increase the mechanical properties of geopolymer composites [16]. Flax and wool fibres have also shown positive effects when used in geopolymer composites. These fibres improved the fracture and mechanical properties of these composites [17, 18].

Researchers of polymers and ceramics have recently become interested in nanotechnology, particularly in developing nanocomposites, which have superior physical and mechanical properties. A number of nano-particles are being added to geopolymers to increase mechanical properties. For instance, nano-alumina and nano-silica have been used effectively as reinforcements for geopolymer pastes, providing outstanding mechanical properties. The nanoparticles not only performed as voids-fillers, but also enhanced the geopolymer reaction [19]. In another study, it has been found that nano-silica and nano-alumina particles have the ability to reduce the porosity and water absorption of geopolymer matrices [20]. A further study on the effect of addition of carbon nanotubes to fly-ash-based geopolymer has shown an increase in the mechanical and electrical properties of geopolymer nanocomposites when compared to the control paste [21]. In another study, the addition of calcium carbonate ($CaCO_3$) nanoparticles to high-volume fly-ash concrete improved the flexural and mechanical properties, decreased the porosity and improved the concrete resistance to water absorption [22]. Finally, in a more recent study of

nano-clay cement nano-composites, it was observed that nano-clay not only increased mechanical and physical properties of cement matrices, but also improved thermal properties [23]. However, no research is reported on the effect of nano clay on properties of flax fabric reinforced geopolymer composites.

In this study, the fabrication of eco or "green" nano-composites using nanoclay and flax fibre (FF) as reinforcement of fly ash geopolymer matrices is investigated. Fourier transform infrared spectroscopy (FTIR) and scanning electron microscopy (SEM) are used to investigate the morphology and microstructure of geopolymer/flax nanocomposites. The effect of different nanoclay platelets contents on mechanical properties such as flexural strength and flexural toughness is also evaluated in this paper.

## 1 Experimental Procedures

### 1.1 Materials and preparation

Low calcium fly ash (ASTM class F), collected from the Eraring power station in NSW, was used as the source material for the geopolymer matrix. The chemical composition of fly ash is shown in Table 1. The alkaline activator for geopolymerisation was a combination of sodium hydroxide and sodium silicate grade D solution. Sodium hydroxide flakes of 98% purity were used to prepare the solution. The chemical composition of sodium silicate used was 14.7% $Na_2O$, 29.4% $SiO_2$ and 55.9% water by mass.

Flax fabric (FF) and organo-nanoclay (Cloisite 30B) were used for the reinforcement of geopolymer nanocomposites. The fabric of 30×30 $cm^2$, supplied by Pure Linen Australia, is made up of yarns with a density of 1.5 $g/cm^3$; the space between the yarns is between 2 and 4 mm, necessary to allow the geopolymer matrix to penetrate. The average diameter of the fibre yarns was 0.60 mm (Fig. 1a), and the fibres diameter was about 20 μm (see Fig. 1b). The physical properties

of the flax fibres are presented in Table 2. The nanoclay platelets used in this study was based on natural montmorillonite clay ($(Na,Ca)_{0.33}(Al,Mg)_2(Si_4O_{10})(OH)_2.nH_2O$) which was supplied by Southern Clay Products, USA. The description and physical properties of Cloisite 30B are shown in Table. 3 [24].

To prepare the geopolymer matrix, an alkaline solution to fly ash ratio of 0.75 was used and the ratio of sodium silicate solution to sodium hydroxide solution was fixed at 2.5. The concentration of sodium hydroxide solution was 8 M, and was prepared and combined with the sodium silicate solution one day before mixing.

The nanoclay was added first to the fly ash at the dosages of 0%, 1.0%, 2.0% and 3.0% by weight. The fly ash and nanoclay were dry mixed for 5 min in a covered mixer at a low speed and then mixed for another 10 min at high speed until homogeneity was achieved. The alkaline solution was then added slowly to the fly ash/nanoclay in the mixer at a low speed until the mix became homogeneous, then further mixed for another 10 min on high speed. The resultant mixture was then poured into wooden moulds and placed on a vibration table for two minutes.

Similar mixtures were prepared to produce the nanocomposites reinforced with FF. Four samples of geopolymer pastes reinforced with 4.1 wt% FF were prepared by spreading a thin layer of geopolymer paste in a well-greased wooden mould and carefully placing the first layer of FF on it. The fabric was fully saturated with paste by a roller, and the process repeated for ten layers; each specimen contained a different weight percentage of nanoclay. The samples then were left under heavy weight for 1 hour to reduce entrapped air inside the samples. All samples were covered with plastic film and cured at 80℃ for 24 hours in an oven before demoulding. They were then dried under ambient conditions for 28 days. The pure geopolymer, and nanocomposites containing 1.0%, 2.0% and 3.0% nanoclay were labeled as GP, GPNC-1, GPNC-2 and GPNC-3, respectively. Also,

the composites reinforced with a combination of FF and the same weight percentages of nanoclay were denoted as GPFNC-0, GPFNC-1, GPFNC-2 and GPFNC-3, respectively (see Table 4).

### 1.2 Mechanical properties

A LLOYD Material Testing Machine (50kN capacity) with a displacement rate of 1 mm/min was used to perform the mechanical tests. Rectangular bars of 60×18×15 $mm^3$ with a span of 40mm were cut from the fully cured samples for three-point bend tests to evaluate the mechanical properties. All samples were aligned horizontally to the applied load in all mechanical tests. Five samples of each composite were used to evaluate the flexural strength according to the standard ASTM D790 [25]. The values were recorded and analysed with the machine software (NEXYGENPlus) and average values were calculated. The flexural toughness of the composites containing FF were characterised by the toughness indices $I_5$, $I_{10}$ and $I_{failure}$ as defined by ASTM C1018 [26].

### 1.3 Characterisation

The samples were measured on a D8 Advance Diffractometer (Bruker-AXS) using copper radiation and a LynxEye position sensitive detector. The diffractometer were scanned from 7° to 60° (2θ) in steps of 0.015° using a scanning rate of 0.5°/min. XRD patterns were obtained by using Cu $K_\alpha$ lines (λ = 1.5406 Å).

An FTIR spectrum was performed on a Perkin Elmer Spectrum 100 FTIR spectrometer in the range of 4000–500 $cm^1$ at room temperature. The spectrum was an average of 10 scans at a resolution of 2 $cm^{-1}$, corrected for background.

The microstructures of geopolymer composites were examined using a Zeiss Neon focused ion beam scanning electron microscope (FIB–SEM), equipped with energy dispersive spectroscopy (EDS). The specimens were mounted on aluminium stubs using carbon tape and then coated with a thin layer of platinum to prevent charging before the observation.

## 2 Results and Discussion

### 2.1 Physical properties

The results of porosity and water absorption of all samples are shown in Fig. 2. It can be seen in general that the composites containing FF have higher porosity and water absorption than those composites without FF. This is because of the hydrophilic nature of cellulose fibres, which creates voids in the interfacial region between the flax fibres and the matrices [27].

All geopolymer nanocomposites displayed higher densities and lower porosities than the control paste. This indicates that nanoclay particles played a pore-filling role to reduce the porosity of the geopolymer composites, producing dense geopolymer paste. As a consequence of this, the geopolymer nanocomposites exhibited lower water absorption. The optimum addition was found as 2.0 wt% of nanoclay, which reduced the porosity by 7.1%, and the water absorption by 17% when compared to the pure geopolymer matrix. However, the addition of excessive amounts of nanoclay increased the porosity and water absorption, and decreased the density of the nanocomposite sample due to the poor dispersion and agglomeration of nanoparticles [28]. This is a common phenomenon for nanoparticles due to small sizes, and high surface area to volume ratio of nanoparticles (van der Waal's force) [29]. Fig. 3 (a and b) shows SEM images of agglomerated nanoclay particles in GPNC-3 sample with Energy Dispersive Spectroscopy (EDS) spectra (Fig. 3b), ammonium salt in the nanoclay is identified by carbon and nitrogen elements. The nitrogen element is not detected clearly in the spectra because the nitrogen content is very low. However, the carbon content is clearly detected at 0.25 KeV. This result is comparable with physical

properties where the porosity of cement paste is decreased due to addition of 1.0 wt% of nanoclay to cement paste. Nevertheless, after the addition of more nanoclay to the paste, values of porosities and water absorption have increased because of the effect of nanoparticles agglomeration [30]. Figs. 4a–d show the SEM micrographs of the surface of neat geopolymer and nanocomposites containing 1.0, 2.0, and 3.0 wt% nano-clay. The pure geopolymer matrix has a porous structure with a higher number of non-reacted and partially reacted fly ash particles embedded in the matrix (Fig. 4a). For the 1–3 wt% nano-clay (Fig. 4b–d) less fly ash particles were observed, and the matrix seemed denser when compared to the matrix of the control sample.

In the case of FF reinforced nanocomposites, the physical properties show similar trends to that of the nanocomposites trends. The optimum loading of nanoclay to the composites was found as 2.0 wt% in the case of GPFNC-2, which decreased the value of porosity by 16.3% and water absorption by 19.4% lower than the sample GPFNC-0.

### 2.2 Thermal behaviour

The thermal stability of neat geopolymer and geopolymer nanocomposites was analyzed using thermogravimetric analysis (TGA) and derivative thermograms (DTG). In this investigation, the thermal stability was studied in terms of the weight-loss percentage as a function of temperature in Argon atmosphere. The results are shown in Fig. 5.

The thermograms of the pure geopolymer and the nanocomposites samples display a weight loss from 25 to 225°C due to the evaporation of absorbed water [31]. The neat geopolymer curve shows sharp decrease in this region compared to the nanocomposites curves, which is clearly shown in DTG graph (Fig. 5), where the peak of nanocomposites shifted to higher temperatures compared to the neat geopolymer. GPNC-2 shows the lowest reduction of rate of he weight loss indicating that geopolymer containing 2.0 wt.% nanoclay has the lowest water content compared to the tested samples. This may be attributed to the effect of nanoclay filling the voids, producing denser

matrices. Between 225°C and 525°C, the rate of weight loss for all samples was slow as the physical free water was evaporated. This gradual weight loss is recognized as the de-hydroxylation of the chemically bound silicon-hydroxyl group giving silicon-oxygen group and evaporated water [32].

$$2Si-OH \longrightarrow Si-O-Si+H_2O\uparrow$$

Between 500°C and 700°C the weight loss was slow and attributed to the burning of the remaining coal of fly ash [33]. This is clear specifically above 600°C in DTG curves where a small hump displaying a small change of the weight loss.

The presence of 1.0, 2.0, and 3.0 wt% nanoclay reduced the weight loss of geopolymer from 12.4% to 12.1, 11.5 and 11.8%, respectively, revealing that the highest improvement to thermal stability of geopolymer matrix was 2.0wt% loading of nanoclay. Note that composites reinforced with flax fibres have not been investigated. This is because that TGA technique is very sensitive to the fibre/matrix ratio, which cannot be fixed for all composites containing FF, considering the small weight of the TGA micro-samples and the flax fibres size. However, the main objective of this study is to determine the effect of nanoclay on the physical structure of the geopolymer/nanocomposites matrices.

### 2.3 X-ray diffraction (XRD)

The XRD spectra obtained for nanoclay, flax fibres, fly ash, GPNC-0 and GPNC-3 specimens are presented in Figs. 6a-6b. The crystalline phases were indexed using Powder Diffraction Files (PDFs) from the Inorganic Crystal Structure Database (ISCD).

Fig. 6a shows the diffraction patterns of nanoclay and flax fibres. Three phases have been indexed in the diffraction pattern of nanoclay with the major phase being Cloisite30B [34], and minor

phases of Cristobalite [$SiO_2$] (PDF 00-039-1425) and Quartz [$SiO_2$](PDF 00-047-0718). Cloisite30B consists of Montmorillonite [$(Ca,Na)_{0.3}Al_2(Si,Al)_4O_{10}(OH)_2 \cdot xH_2O$] and the quaternary ammonium salt. Montmorillonite has four major peaks in the XRD pattern, which correspond to 2θ of 4.84 º, 19.74°, 35.12° and 53.98°. The quaternary ammonium salt has four peaks at 2θ of 4.84 º, 9.55º, 24.42º and 29.49º. Note that there is an overlap of peaks at 2θ of 4.84 º for Montmorillonite and quaternary ammonium salt. Both Cristobalite and Quartz has a peak that corresponds to 2θ of 21.99 º and 26.61 º, respectively. The diffraction pattern of flax fibers shows typical peaks of cellulose (PDF 00-060-1502).

For fly ash, GP and GPNC-3 samples, two major phases are identified clearly: quartz [$SiO_2$] (PDF 00-046-1045) and mullite [$Al_{1.272}\ Si_{0.278}\ O_{4.864}$] (PDF 01-083-1881) (Fig. 6b). As the crystalline phases of quartz and mullite are also the fly ash phases they are insensitive to geopolymetric reactions, and their role is limited in geopolymer paste as filler particles [35, 36]. However, the amorphous aluminosilicate phase that created between $2\theta$ = 14° and 27° is an active indication of geopolymer reaction, which is the reactive and dissolvable content in alkaline solution throughout the geopolymer formation [37]. The geopolymer matrix mechanical properties are noticeably affected through the amorphous phase. When the amorphous phase is higher, the strength of the geopolymer is likewise higher [38, 39]. Fig. 7 shows overlays of the amorphous hump under the quartz phase of nanocomposites samples. It can be seen that GPNC-2 has the highest amorphous phase over all nanocomposites. Also, it can be noticed that GPNC-2 displays less intensity of quartz peak compared to other samples, which demonstrates that the reaction of geopolymer is activated by the optimum addition of nanoclay and higher content of quartz is dissolved, resulting in more geopolymer gel. This improves the mechanical properties of the geopolymer nanocomposites by improving the physical properties of the matrix, besides improving the adhesion between the

reinforcement flax fibres and the matrix. However, the more addition of nanoclay is inactive and resulted in almost the same amount of amorphous content as GPNC-1.

### 2.4 FTIR observation

FTIR spectra of pure geopolymer, nanocomposites, GPF and GPFNC-2 are shown in Figs. 8a and 8b. The strong peak at ~1000 $cm^{-1}$ in all samples is associated with Si-O-T (T: Si or Al) asymmetric stretching vibrations and is the special mark of the geopolymerisation [40]. The level of geopolymerization can be identified quantitatively by comparing the height and the area under the geopolymer stretching peaks of the nanocomposites to the pure matrix peak [33]. Considering the size of the geopolymer peak, it can be seen that all nanocomposites had generally higher contents of geopolymer compared to the control paste (Fig. 8a); however, the addition of 2.0 wt.% of nanoclay had the highest level of geopolymerization among all samples. The areas under the geopolymer peak for the nanocomposites when compared to the pure matrix have enlarged by 2.0%, 7.0% and 3.0%, while the peak's heights have expanded by 2.0%, 19% and 15% for GPNC-1, GPNC-2 and GPNC-3, respectively. This result is in agreement with the XRD results that discussed above. A broad peak at the region of 3200-3600 $cm^{-1}$ is corresponding to the stretching vibration of the hydroxyl (OH) group of physically free water (higher frequencies), and to chemically bounded water to the inorganic polymer through hydrogen bonds (lower frequencies) [24, 41]. The peak around 1640 $cm^{-1}$ is also due to the (OH) bending vibration of absorbed water [33].

Fig. 8b shows the FTIR scan for GPFNC-0 and GPFNC-2. The presence of flax fibres in the samples can be recognised in the peak at 1420 $cm^{1}$, which is attributed to the $CH_2$ bending vibration of cellulose [24]. The intensity of the band at 3200-3600 $cm^{-1}$ is a sign to the samples water uptake. Samples reinforced with FF have higher water uptake because of the hydrophilic nature of cellulose

fibres; however, GPFNC-2 has lower content of water compared to GPFNC-0 due to the barrier property of the nanocomposites against moisture uptake.

### 2.5 Mechanical properties

Flexural tests are used to characterise the mechanical properties of layered composites as they provide a simple means of determining the bending response. This provides useful information on the performance of layered fabric-based composites. The effect of nanoclay contents on the flexural strength of the geopolymer FF-composites is presented in Fig. 9. It can be seen clearly that all composites reinforced with FF showed higher flexural strength than the pure geopolymer and nanocomposites samples. The flexural strength of the composites improved from 4.5 MPa in the control sample to about 23 MPa in GPFNC-0. This result is comparable with that of short flax fibre-reinforced geopolymer composites reported by Alzeer and MacKenzie [17]. This can be explained by the fact that flax fabrics bridge the cracks of geopolymer matrix develop during bending and resisted the failure through frictional deboning of fabric in the matrix. This permits more stress transfer between the matrix and the flax fibres, resulting in greater flexural strength [42].

The addition of nanoclay, however, enhanced the adhesion force between the matrix and fibres creating composites with higher flexural strength. Fig.9 shows that GPFNC-2 had the highest flexural strength among all samples, which means that the optimum addition that improved the flexural strength was 2.0 wt% of nanoclay. The loading of 2.0 wt% not only enhanced the bond between the matrix and the fibre, but also created a denser geopolymer paste with higher contents of geopolymer products.

This result is also confirmed by studying the flexural toughness indices $I_5$, $I_{10}$ and $I_{failure}$ of the composites (Fig. 10a). According to the standard used, $I_5$ is defined as the ratio obtained by dividing

the area up to a deflection of three times the first-crack deflection by the area up to first crack, while $I_{10}$ is the ratio between the area up to a deflection of 5.5 times the first-crack deflection by the area up to the first crack. For the failure deflection, $I_{failure}$ is calculated at 11.4 mm deflection for all samples reinforced with FF.

Pure geopolymer and geopolymer nanocomposites had zero values of toughness because of the brittleness of the geopolymer. However, FF-reinforced composites exhibited high flexural toughness due to the ability of long fibres to withstand a higher load and to support multiple cracks throughout the loading process, which prevented the brittle failure of geopolymer.

Fig. 10b presents values of toughness indices of FF-reinforced composites, the sample reinforced with the optimum loading of nanoclay showed higher toughness indices than GPFNC-0 by 58%, 54% and 39% for $I_5$, $I_{10}$ and $I_{failure}$, respectively. The rate of improvement of the toughness indices decreased with deflection. While $I_5$ has enhanced by 58% after the addition of 2.0 wt% of nanoclay, $I_{failure}$ has only improved by 39%. This may be attributed to the effect of fibre pull-out that occurred more extensively in GPFNC-0 than in GPFNC-2. The bond between the matrix and flax fibres has improved due to the high content of geopolymer gel, which caused more fibres fracture than the pull-out in GPFNC-2. This can be considered clearly in Fig. 10a, where the slope of GPFNC-2 curve has sharper decrease in load with increasing deflection in the region between 9 and 11 mm than other curves.

SEM images of the fracture surface of FF-reinforced geopolymer composite and FF-reinforced nanocomposites after flexural toughness test are shown in Figs. 11. A range of toughness mechanisms such as fibre de-bonding, fibre pull-out and rupture and matrix fracture can be clearly seen. The examination of fracture surface of FF reinforced geopolymer composite shows high porous structure and number of unreacted fly ash, which caused poor adhesion between fibres and the matrix (Fig. 11a). FF-reinforced nanocomposites containing 1.0 and 3.0wt% nanoclay displays

relatively denser matrices with lower number of unreacted fly ash particles embedded in the matrices (Figs. 11b and 11d). However, in FF-reinforced geopolymer nanocomposite containing 2.0 wt% nanoclay, a smaller amount of unreacted fly ash particles was observed, and higher content of geopolymer gel can be clearly seen, which provided better adhesion between the flax fibres and the matrix. A significant amount of fibre fracture was also observed (Fig. 11c) by virtue of this enhanced interfacial fibre-matrix bonding.

## 2.6 Conclusions

The investigation of FF-reinforced geopolymer nanocomposites and the effects of nanoclay through physical and mechanical testing presented a number of findings. Analysis using FTIR and XRD show that nanocomposites of geopolymer with the optimum amount of nanoclay produce higher amounts of geopolymer gel. The nanoclay added to nanocomposites at 2.0 wt% provides a denser microstructure, and has better adhesion bond between the matrix and the flax fibres. It was also observed that the loading of 2.0 wt% nanoclay to the nanocomposites reduced the porosity and increased the density; this caused an improvement in flexural strength and toughness. However, adverse physical and mechanical properties are observed when the FF-reinforced geopolymer contains nanoclay loadings that exceeded the 2.0 wt%.

## Acknowledgments

The authors would like to thank Ms E. Miller from the Department of Applied Physics at Curtin University for her assistance with SEM. The author (HA) is grateful to the Physics Department of Umm Al-Qura University for the financial support in the form of a PhD scholarship.

**References**

[1] Barbosa VFF, MacKenzie KJD, Thaumaturgo C. Synthesis and characterisation of materials based on inorganic polymers of alumina and silica: sodium polysialate polymers. Inter J Inorg Mater. 2000;2(4):309-17.

[2] van-Jaarsveld JGS, van-Deventer JSJ, Lorenzen L. Factors Affecting the Immobilization of Metals in Geopolymerized Flyash. Metal Mater Trans. 1998;29B(291).

[3] Davidovits J. Geopolymers and geopolymeric materials. J Therm Anal. 1989;35(2):429-41.

[4] Duxson P, Fernández-Jiménez A, Provis JL, Lukey GC, Palomo A, Deventer JSJ. Geopolymer technology: the current state of the art. J Mater Sci. 2007;42(9):2917-33.

[5] Pernica D, Reis PNB, Ferreira JAM, Louda P. Effect of test conditions on the bending strength of a geopolymer- reinforced composite. J Mater Sci. 2010;45(3):744-9.

[6] Lin T, Jia D, He P, Wang M, Liang D. Effects of fiber length on mechanical properties and fracture behavior of short carbon fiber reinforced geopolymer matrix composites. Mater Sci Eng, A. 2008;497(1-2):181-5.

[7] Alomayri T, Shaikh FUA, Low IM. Synthesis and mechanical properties of cotton fabric reinforced geopolymer composites. Compos Part B. 2014;60:36-42.

[8] Bernal SA, Bejarano J, Garzón C, Mejía de Gutiérrez R, Delvasto S, Rodríguez ED. Performance of refractory aluminosilicate particle/fiber-reinforced geopolymer composites. Compos Part B. 2012;43(4):1919-28.

[9] Herrera-Franco PJ, Valadez-González A. A study of the mechanical properties of short natural-fiber reinforced composites. Compos Part B. 2005;36(8):597-608.

[10] Bohlooli H, Nazari A, Khalaj G, Kaykha MM, Riahi S. Experimental investigations and fuzzy logic modeling of compressive strength of geopolymers with seeded fly ash and rice husk bark ash. Compos Part B. 2012;43(3):1293-301.

[11] Low IM, Somers J, Pang WK. Synthesis and Properties of Recycled Paper-Nano-Clay-Reinforced Epoxy Eco-Composites. Key Eng Mater. 2007;334:609-12.

[12] Zadorecki P, Michell A. Future-prospect for wood cellulose as reinforcment in otganic polymer composites. Polym Compos. 1989;10(2):69-77.

[13] Low IM, Somers J, Kho HS, Davies IJ, Latella BA. Fabrication and properties of recycled cellulose fibre-reinforced epoxy composites. Compos Interfaces. 2009;16(7-9):659-69.

[14] Rahman MM, Rashid MH, Hossain MA, Hasan MT, Hasan MK. Performance Evaluation of Bamboo Reinforced Concrete Beam. Int J Eng Tech. 2011;11(04):142-6.

[15] Lin X, Silsbee MR, Roy DM, Kessler K, Blankenhorn PR. Approaches to improve the properties of wood fiber reinforced cementitious composites. Cem Concr Res. 1994;24(8):1558-66.

[16] Alomayri T, Shaikh FUA, Low IM. Characterisation of cotton fibre-reinforced geopolymer composites. Compos Part B. 2013;50:1-6.

[17] Alzeer M, MacKenzie K. Synthesis and mechanical properties of novel composites of inorganic polymers (geopolymers) with unidirectional natural flax fibres (phormium tenax). Appl Clay Sci. 2013;75-76:148-52.

[18] Alzeer M, MacKenzie KD. Synthesis and mechanical properties of new fibre-reinforced composites of inorganic polymers with natural wool fibres. J Mater Sci. 2012;47(19):6958-65.

[19] Phoo-ngernkham T, Chindaprasirt P, Sata V, Hanjitsuwan S, Hatanaka S. The effect of adding nano-SiO2 and nano-Al2O3 on properties of high calcium fly ash geopolymer cured at ambient temperature. Mater Des. 2014;55:58-65.

[20] Nazari A, Sanjayan JG. Hybrid effects of alumina and silica nanoparticles on water absorption of geopolymers: Application of Taguchi approach. Measurement. 2015;60:240-6.

[21] Saafi M, Andrew K, Tang PL, McGhon D, Taylor S, Rahman M, et al. Multifunctional properties of carbon nanotube/fly ash geopolymeric nanocomposites. Constr Build Mater. 2013;49:46-55.

[22] Shaikh FUA, Supit SWM. Mechanical and durability properties of high volume fly ash (HVFA) concrete containing calcium carbonate (CaCO3) nanoparticles. Constr Build Mater. 2014;70:309-21.

[23] Hakamy A, Shaikh FUA, Low IM. Characteristics of nanoclay and calcined nanoclay-cement nanocomposites. Compos Part B. 2015;78:174-84.

[24] Alamri H, Low IM. Effect of water absorption on the mechanical properties of nanoclay filled recycled cellulose fibre reinforced epoxy hybrid nanocomposites. Compos Part A. 2013;44:23-31.

[25] ASTM. Standard Test Methods for Flexural Properties of Unreinforced and Reinforced Plastics and Electrical Insulating Materials. 2010.

[26] ASTM. Standard Test Method for Flexural Toughness and First-Crack Strength of Fiber-Reinforced Concrete (Using Beam With Third-Point Loading). 1998.

[27] Alomayri T, Assaedi H, Shaikh FUA, Low IM. Effect of water absorption on the mechanical properties of cotton fabric-reinforced geopolymer composites. Journal of Asian Ceramic Societies. 2014.

[28] Alamri H, Low IM, Alothman Z. Mechanical, thermal and microstructural characteristics of cellulose fibre reinforced epoxy/organoclay nanocomposites. Compos Part B. 2012;43(7):2762-71.

[29] Shaikh F, Supit S, Sarker P. A study on the effect of nano silica on compressive strength of high volume fly ash mortars and concretes. Mater Des. 2014;60:433-42.

[30] Hakamy A, Shaikh FUA, Low IM. Thermal and mechanical properties of hemp fabric-reinforced nanoclay–cement nanocomposites. Journal of Materials Science. 2013.

[31] Zivica V, Palou MT, Bage TIL. High strength metahalloysite based geopolymer. Compos Part B. 2014;57:155-65.

[32] Li Q, Xu H, Li F, Li P, Shen L, Zhai J. Synthesis of geopolymer composites from blends of CFBC fly and bottom ashes. Fuel. 2012;97:366-72.

[33] ul-Haq E, Kunjalukkal Padmanabhan S, Licciulli A. Synthesis and characteristics of fly ash and bottom ash based geopolymers–A comparative study. Ceram Int. 2014;40(2):2965-71.

[34] Ebadi-Dehaghani H, Khonakdar HA, Barikani M, Jafari SH. Experimental and theoretical analyses of mechanical properties of PP/PLA/clay nanocomposites. Compos Part B. 2015;69:133-44.

[35] Fernandez-Jimenez A, Palomo A. Composition and microstructure of alkali activated fly ash binder: Effect of the activator. Cem Concr Res. 2005;35(10):1984-92.

[36] Alomayri T, Low IM. Synthesis and characterization of mechanical properties in cotton fiber-reinforced geopolymer composites. Journal of Asian Ceramic Societies. 2013;1(1):30-4.

[37] Chen-Tanw N, van-Riessen A. Determining the Reactivity of a Fly Ash for Production of Geopolymer. J Am Ceram Soc. 2009;92:881-7.

[38] Bakharev T. Thermal behaviour of geopolymers prepared using class F fly ash and elevated temperature curing. Cem Concr Res. 2006;36(6):1134-47.

[39] Rickard WDA, Williams R, Temuujin J, van Riessen A. Assessing the suitability of three Australian fly ashes as an aluminosilicate source for geopolymers in high temperature applications. Mater Sci Eng: A. 2011;528(9):3390-7.

[40] Phair JW, van-Deventer JSJ. Effect of the silicate activator pH on the microstructural characteristics of waste-based geopolymers. Int J Miner Process. 2002;66(1-4):121-43.

[41] Kanny K, Mohan TP. Resin infusion analysis of nanoclay filled glass fiber laminates. Compos Part B. 2014;58:328-34.

[42] Sim J, Park C, Moon DY. Characteristics of basalt fiber as a strengthening material for concrete structures. Compos Part B. 2005;36(6-7):504-12.

**Tables:**

Table 1: Chemical compositions of fly ash (wt%).

| $SiO_2$ | $Al_2O_3$ | CaO | $Fe_2O_3$ | $K_2O$ | MgO | $Na_2O$ | $P_2O_5$ | $SO_3$ | $TiO_2$ | MnO | BaO | LOI |
|---|---|---|---|---|---|---|---|---|---|---|---|---|
| 63.13 | 24.88 | 2.58 | 3.07 | 2.01 | 0.61 | 0.71 | 0.17 | 0.18 | 0.96 | 0.05 | 0.07 | 1.45 |

Table 2: Structure and physical properties of the flax fabric (Source of reference?).

| | |
|---|---|
| Fabric thickness (mm) | 0.6 |
| Fabric geometry | Woven (plain weave) |
| Yarn nature | Bundle |
| Bundle diameter (mm) | 0.6 (see Fig. 2a) |
| Filament size (mm) | 0.01-0.02 (see Fig. 2b) |
| Opening size (mm) | 2-4 |
| Fabric density ($g/cm^3$) | 1.5 |
| Modulus of elasticity (GPa) | 39.5 |
| Tensile strength (MPa) | 660 |

Table 3: Physical properties of the organo-nanoclay platelets (Cloisite 30B).

| Colour | Off white |
|---|---|
| Density ($g/cm^3$) | 1.98 |
| d-spacing (001) (nm) | 1.85 |
| Aspect ratio | 200-1000 |
| Surface area ($m^2/g$) | 750 |

Table 4: Formulation of samples.

| Sample name | Fly-ash (g) | NaOH solution (g) | $Na_2SiO_3$ solution (g) | Nanoclay (g) | FF content (wt%) |
|---|---|---|---|---|---|
| GP | 1000 | 214.5 | 535.5 | 0 | 0 |
| GPNC-1 | 1000 | 214.5 | 535.5 | 10 | 0 |
| GPNC-2 | 1000 | 214.5 | 535.5 | 20 | 0 |
| GPNC-3 | 1000 | 214.5 | 535.5 | 30 | 0 |
| GPFNC-0 | 1000 | 214.5 | 535.5 | 0 | 4.1 |
| GPFNC-1 | 1000 | 214.5 | 535.5 | 10 | 4.1 |
| GPFNC-2 | 1000 | 214.5 | 535.5 | 20 | 4.1 |
| GPFNC-3 | 1000 | 214.5 | 535.5 | 30 | 4.1 |

**Figure captions**

1. Diameters of the (a) flax bundle, and (b) flax fibres.
2. Density, porosity and water absorption values for all samples.
3. (a) SEM image of agglomerated nanoclay particles on the fracture surface of GPNC-3, (b) with EDS analysis.
4. SEM images of the fracture surface of geopolymer nanocomposites with different loadings of nano-clay (a) pure geopolymer, (b) 1.0 wt%, (c) 2.0 wt% and (d) 3.0 wt%. [Leged: 1. Pores and 2. Unreacted fly-ash]
5. TGA/DTG curves of pure geopolymer and geopolymer nanocomposites.
6. X-ray diffraction patterns of: (a) nano-clay platelets and flax fibres, (b) fly-ash, GP and GPNC-3.
7. An overlay of the amorphous phases of XRD patterns for pure geopolymer, GPNC-1, GPNC-2 and GPNC-3.
8. (a) FTIR spectra of pure geopolymer and the nanocomposites GPNC-1, GPNC-2 and GPNC-3, (b) FTIR spectra of the FF-reinforced geopolymer composite GPFNC-0 and GPFNC-2.
9. Flexural strength of all samples.
10. (a) Typical load-midspan deflection curves of all composites, (b) Toughness indices $I_5$, $I_{10}$ and $I_{failure}$ for FF/reinforced geopolymer samples.
11. SEM images of a fracture surface of FF-reinforced samples; (a) GPFNC-0, (b) GPFNC-1, (c) GPFNC-2 (d) GPFNC-3.

**1_diameter of FF**

**Click here to download high resolution image**

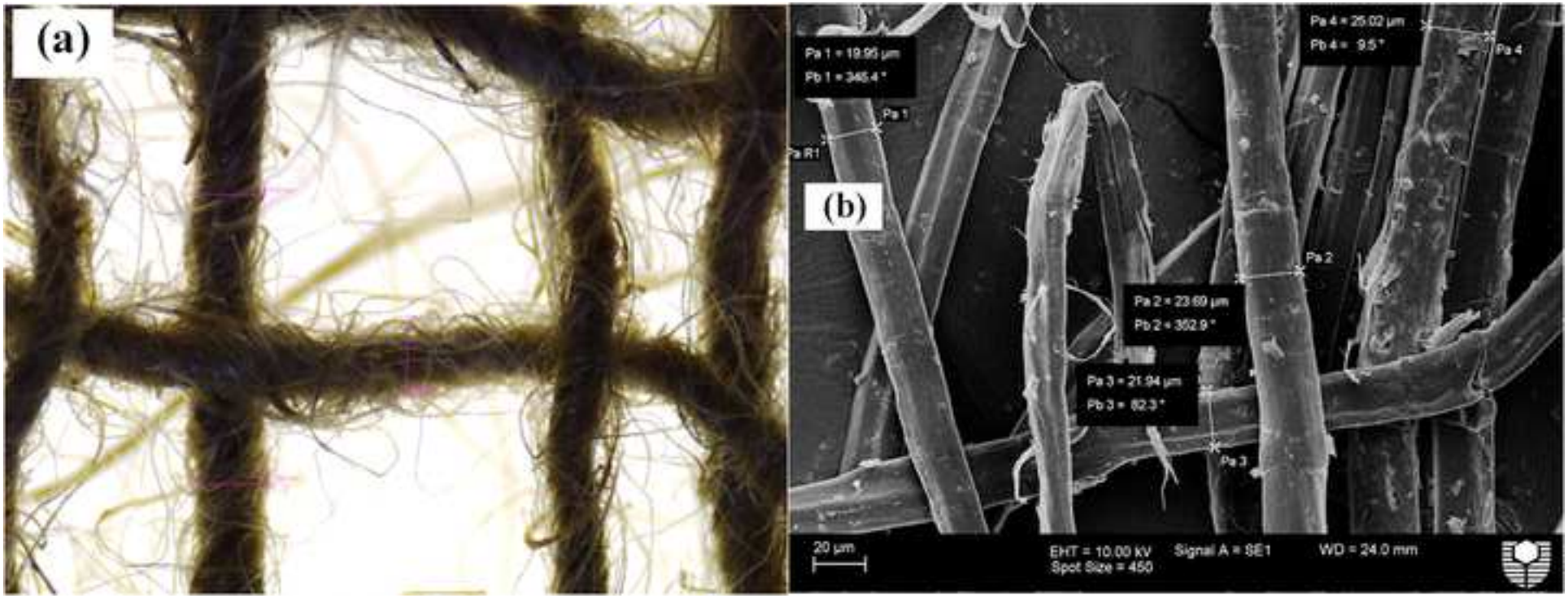

2_PorosityDensityWA

Click here to download high resolution image

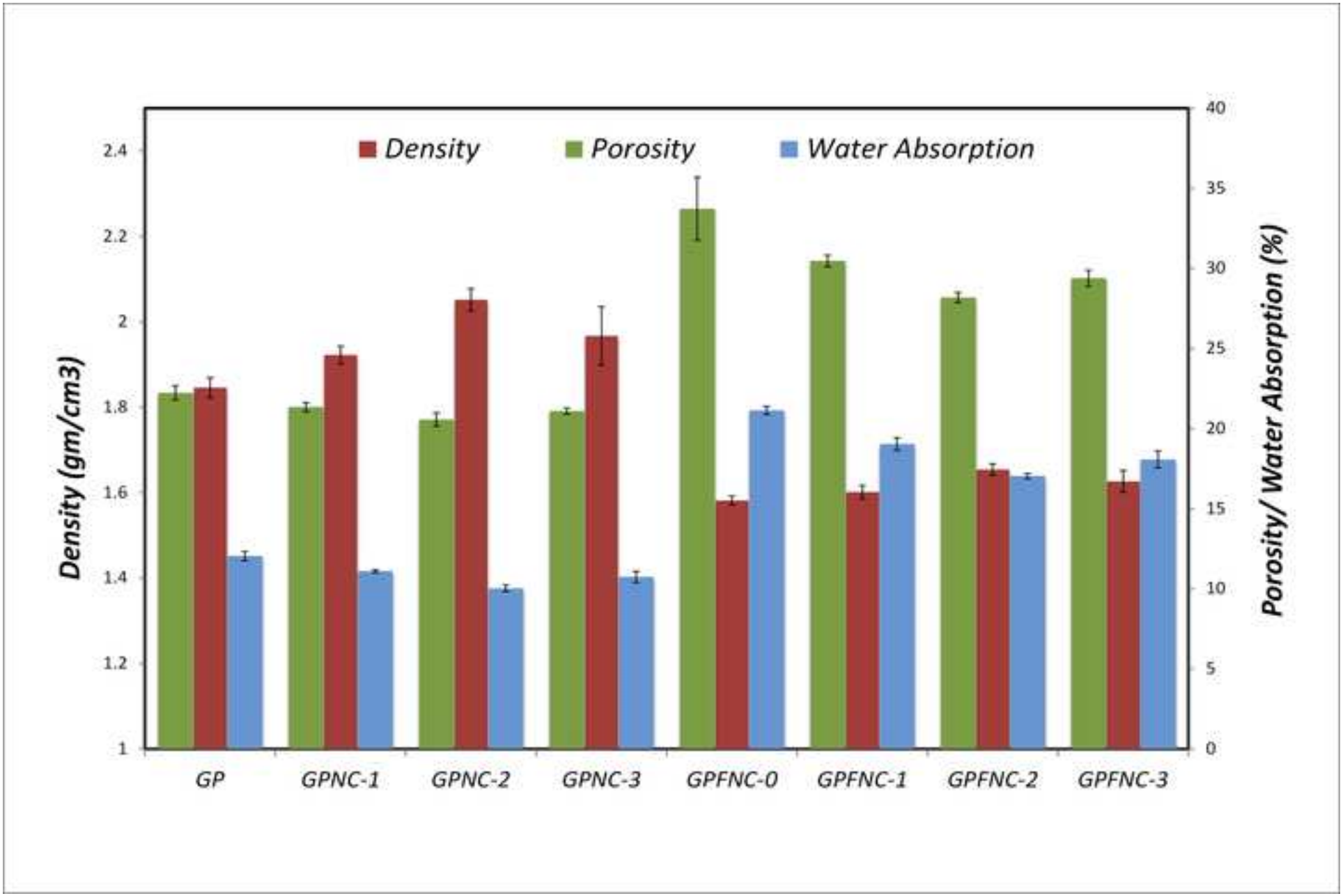

**3a_AgglomerationSEM**

**Click here to download high resolution image**

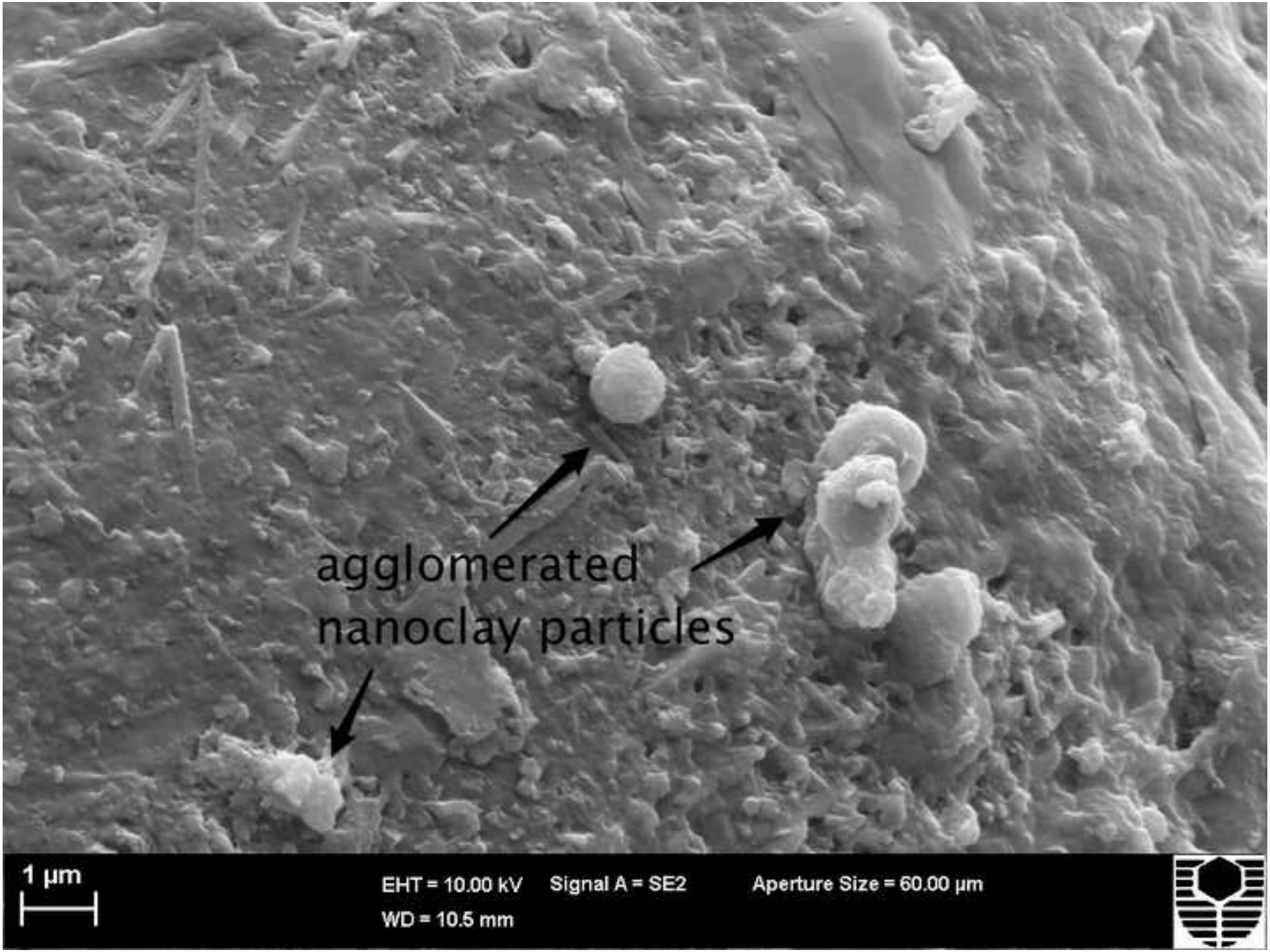

**3b_EDS**

**Click here to download high resolution image**

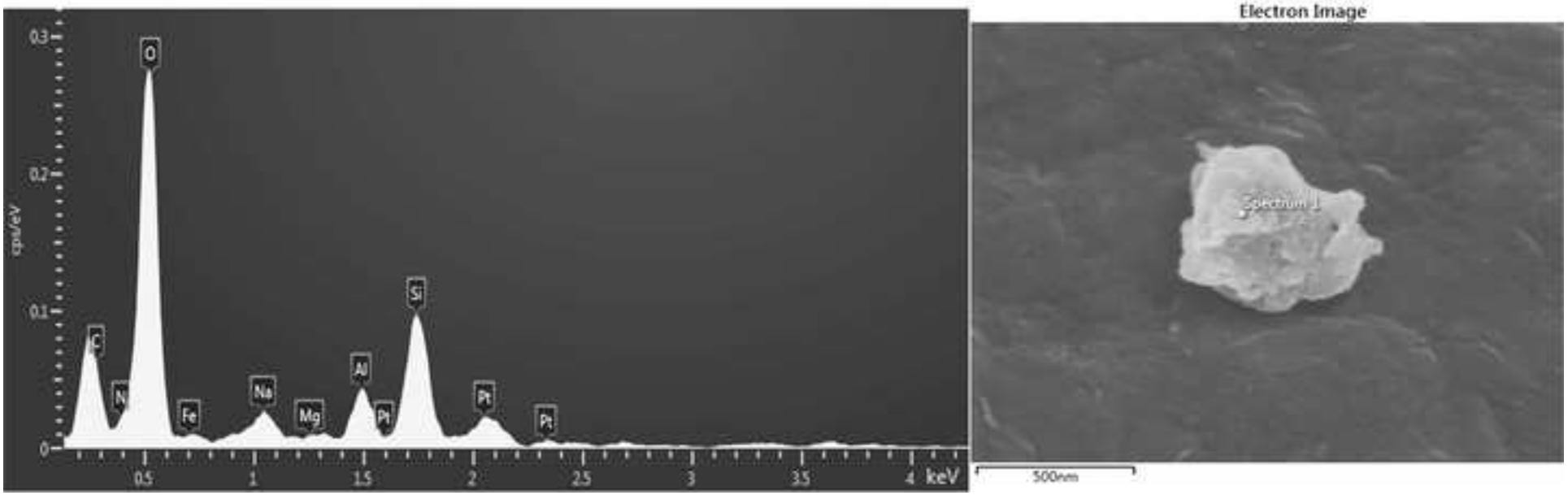

4_a_P

Click here to download high resolution image

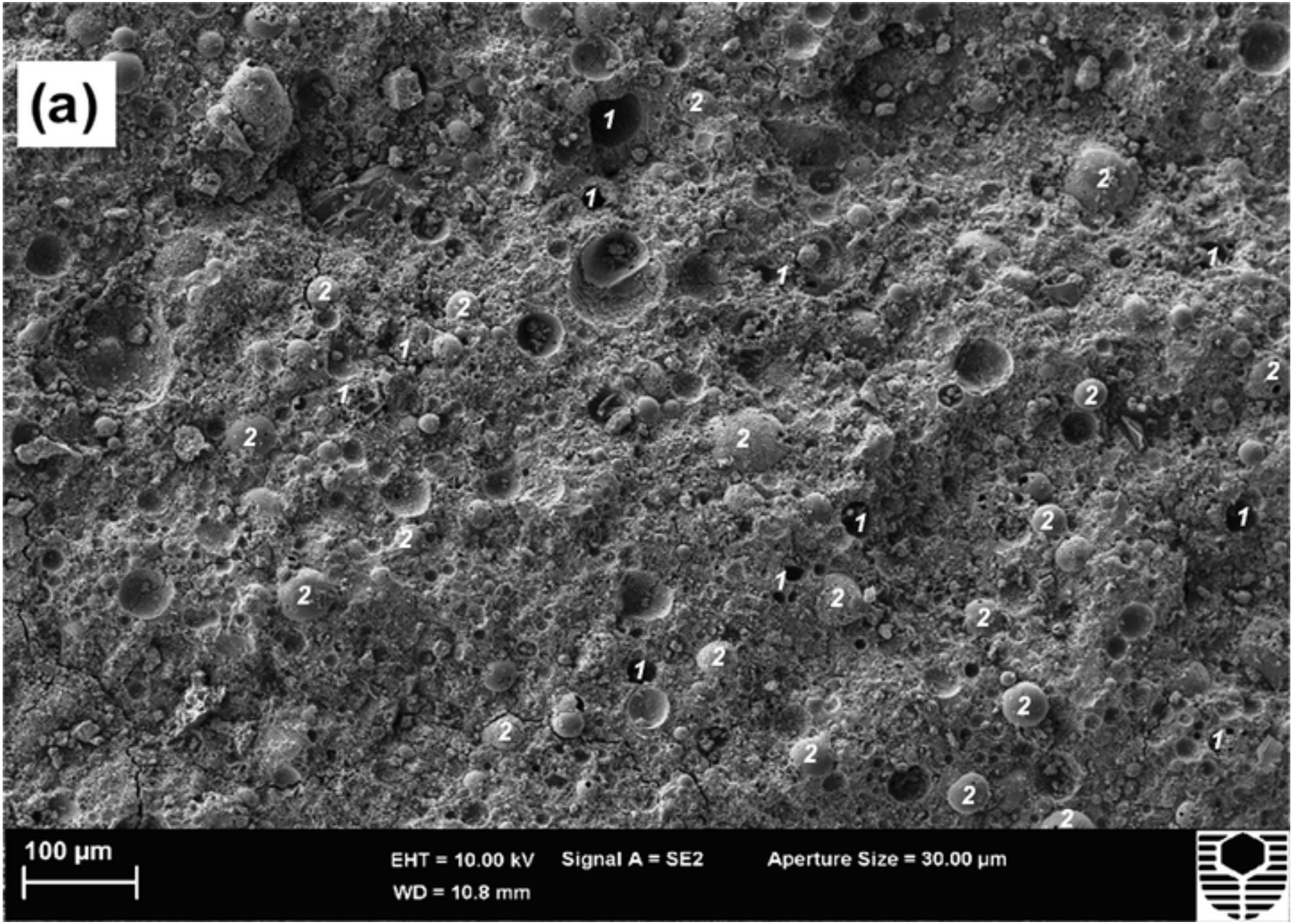

4_b_1NC

Click here to download high resolution image

4_c_2NC

Click here to download high resolution image

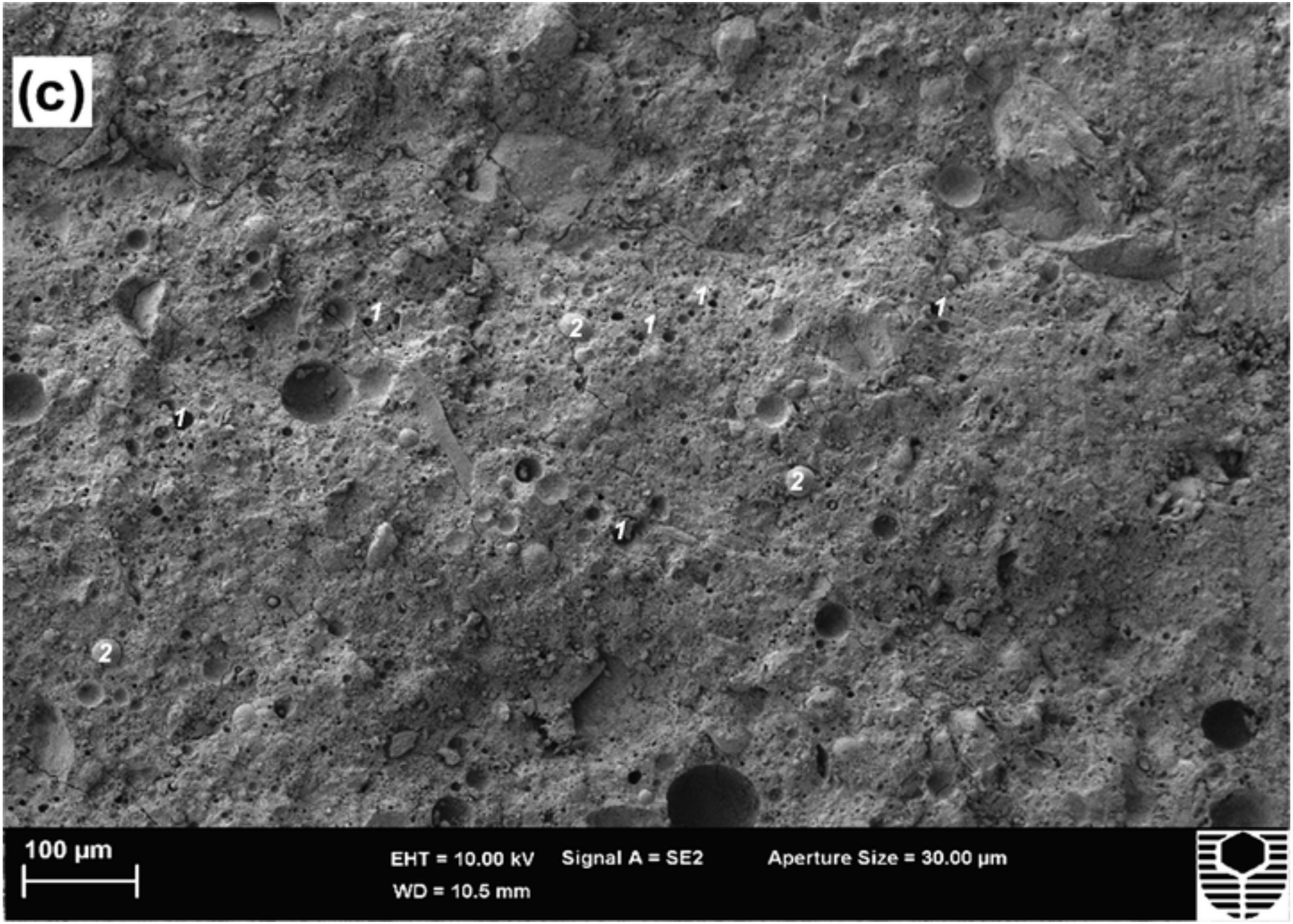

4_d_3NC

Click here to download high resolution image

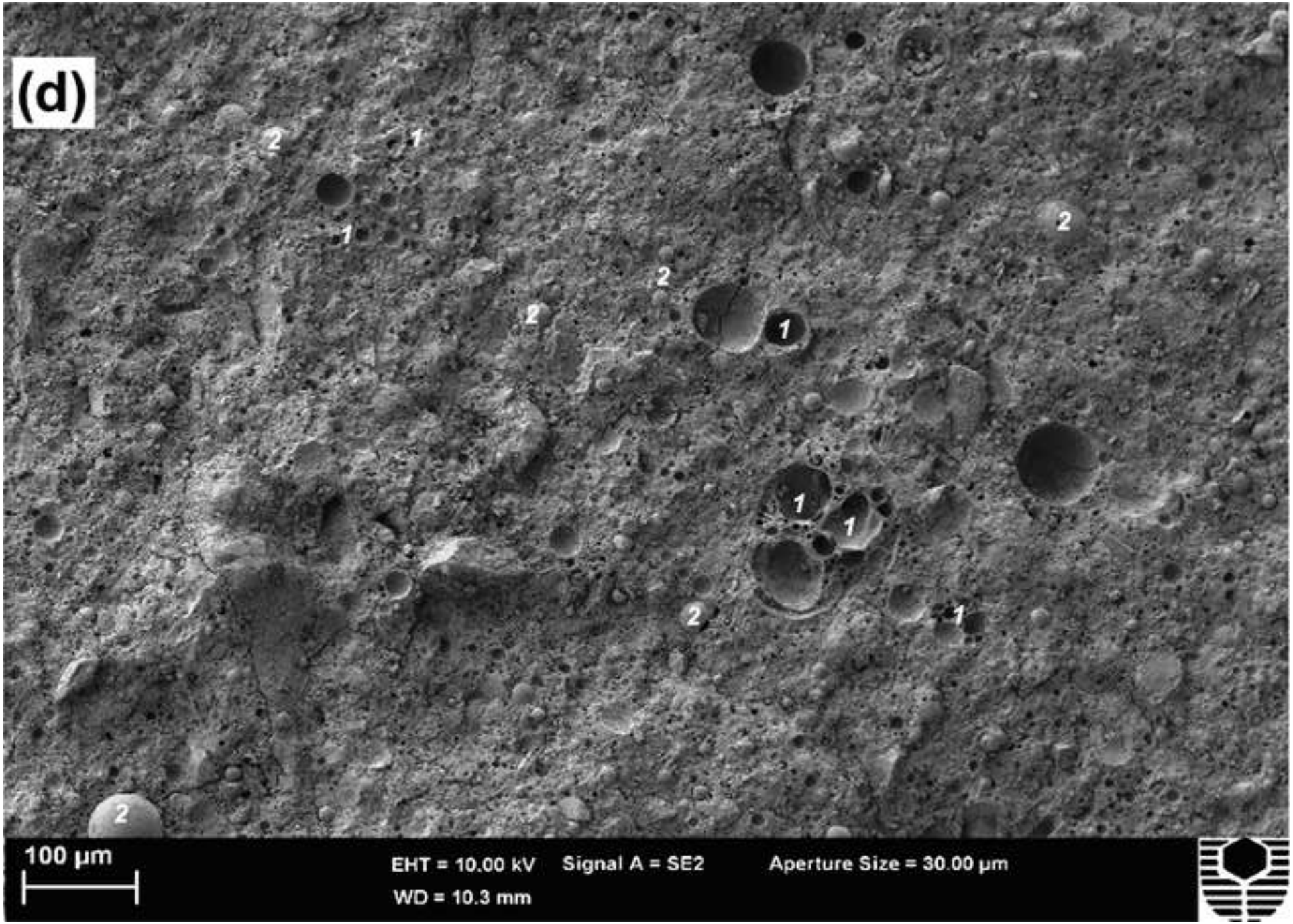

5_TGA-DTG

Click here to download high resolution image

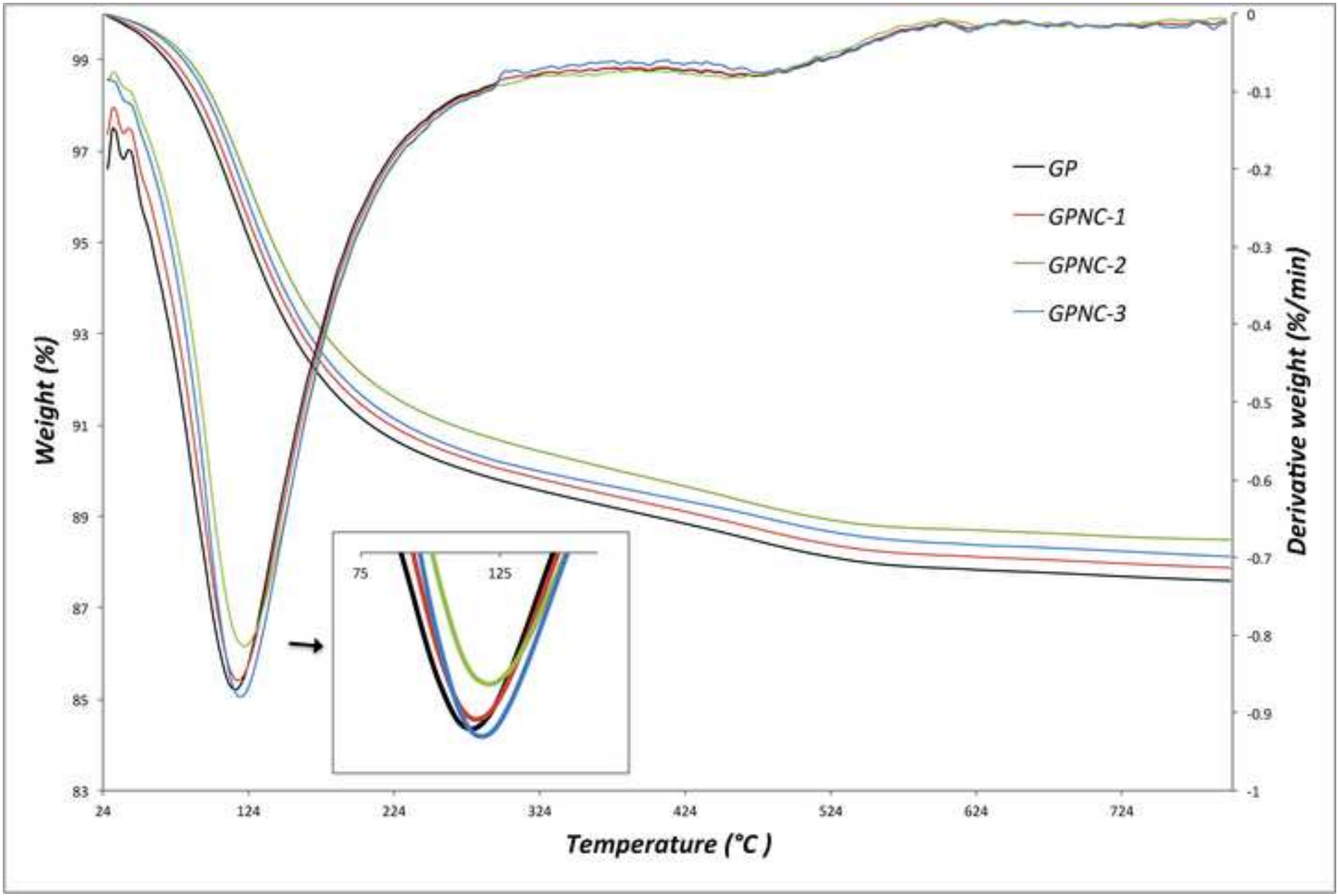

6a_XRD_NC_FF

Click here to download high resolution image

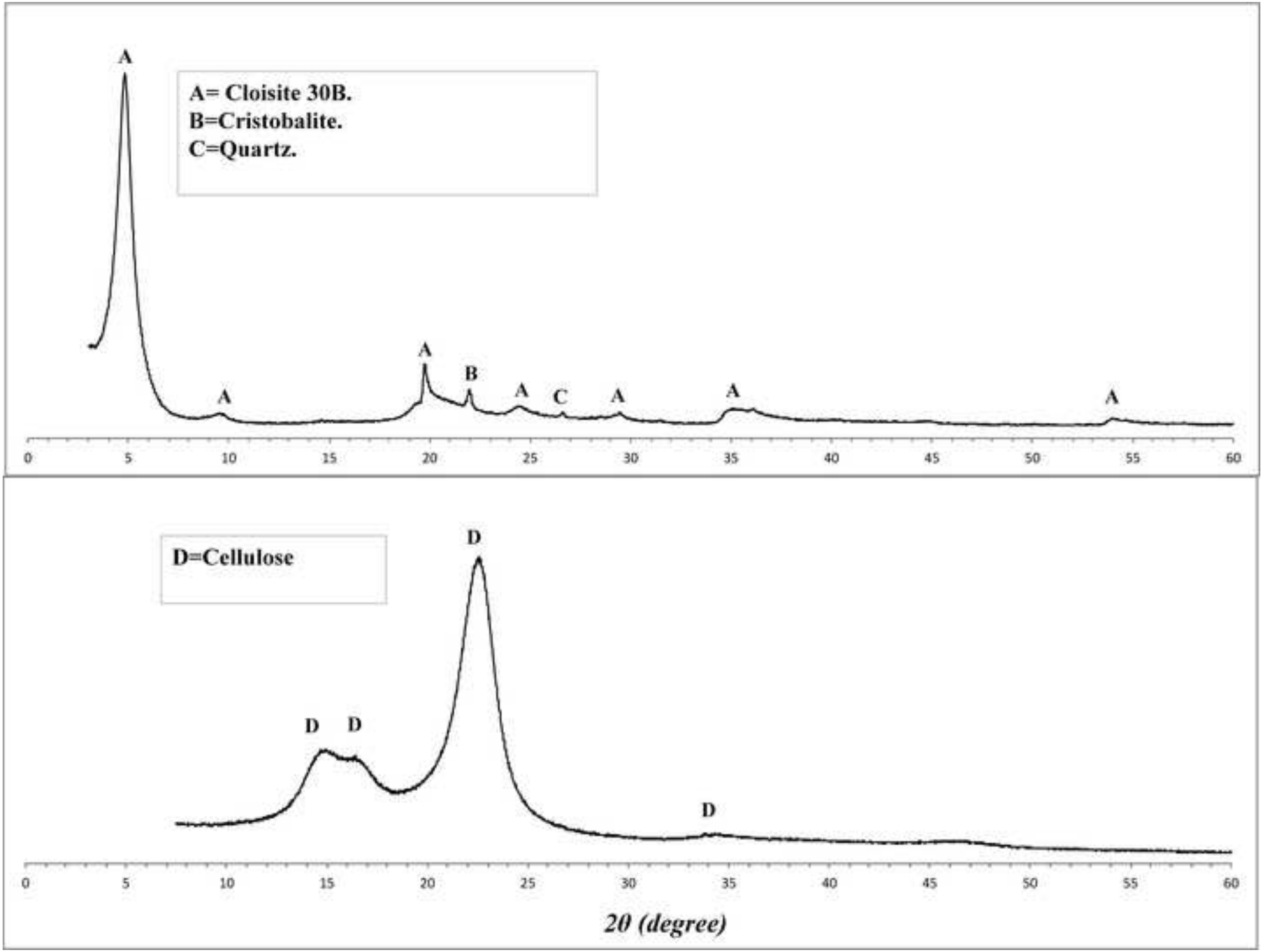

6b_XRD_GP

Click here to download high resolution image

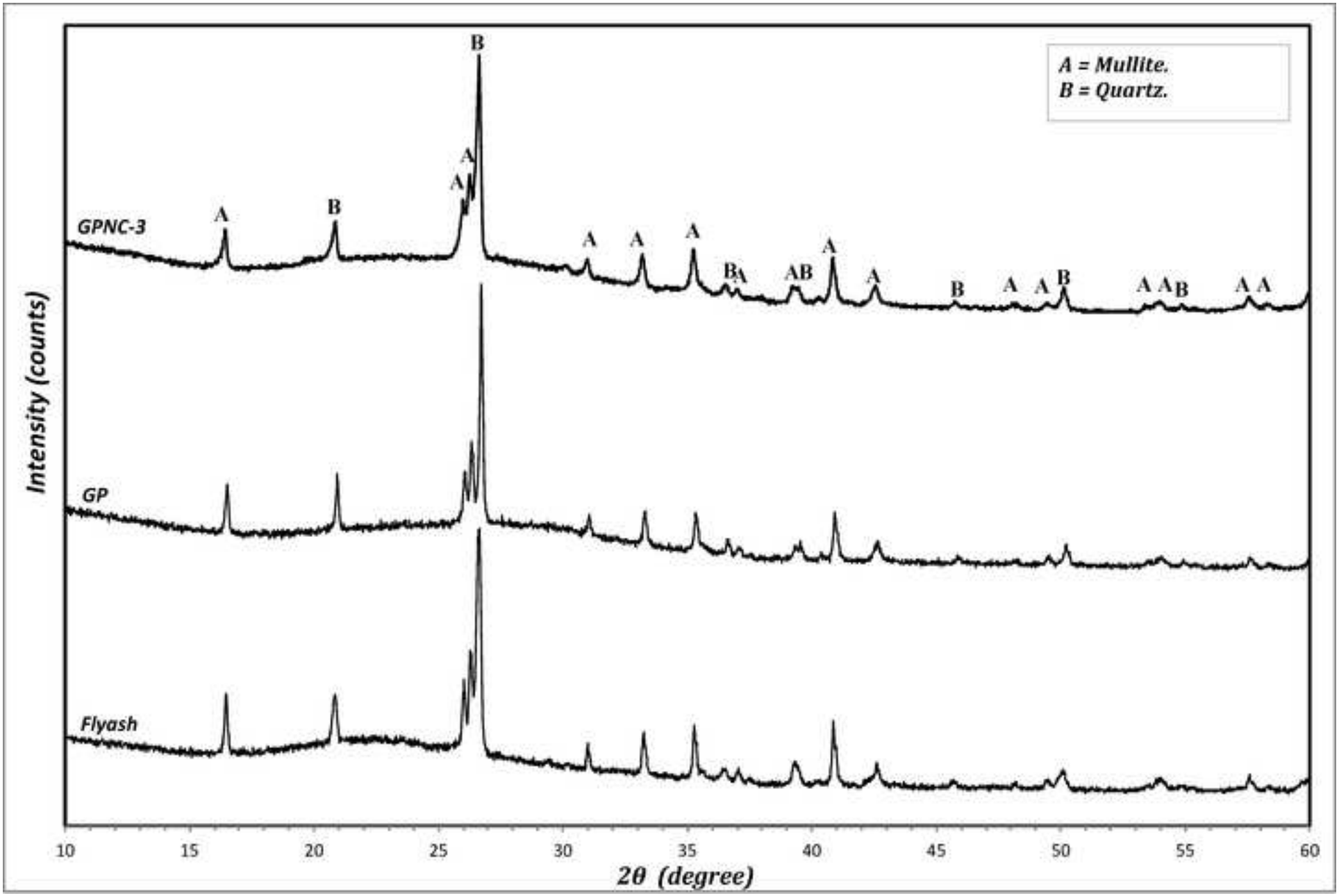

7_XRD_Overlay

Click here to download high resolution image

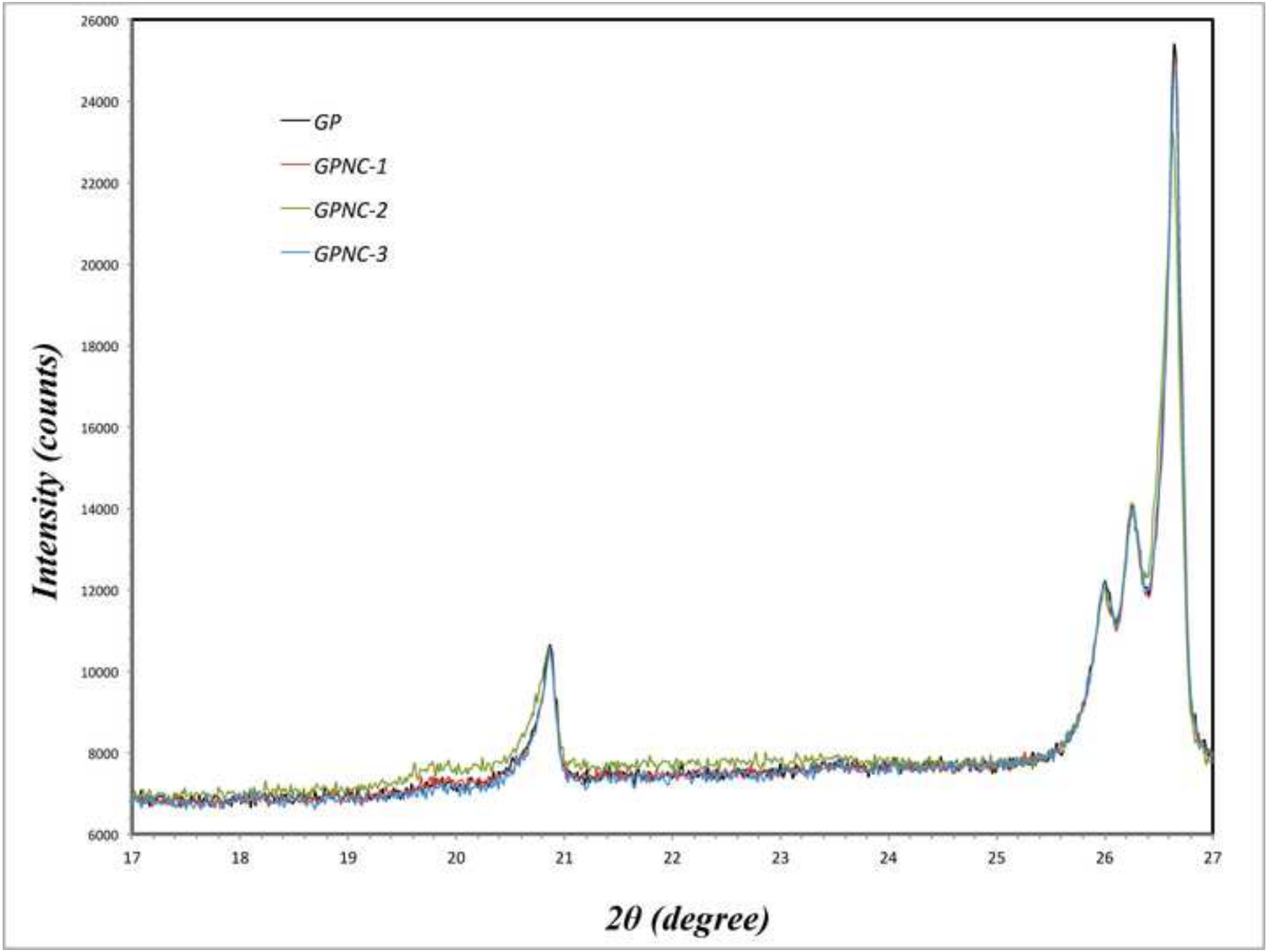

8a_FTIR

Click here to download high resolution image

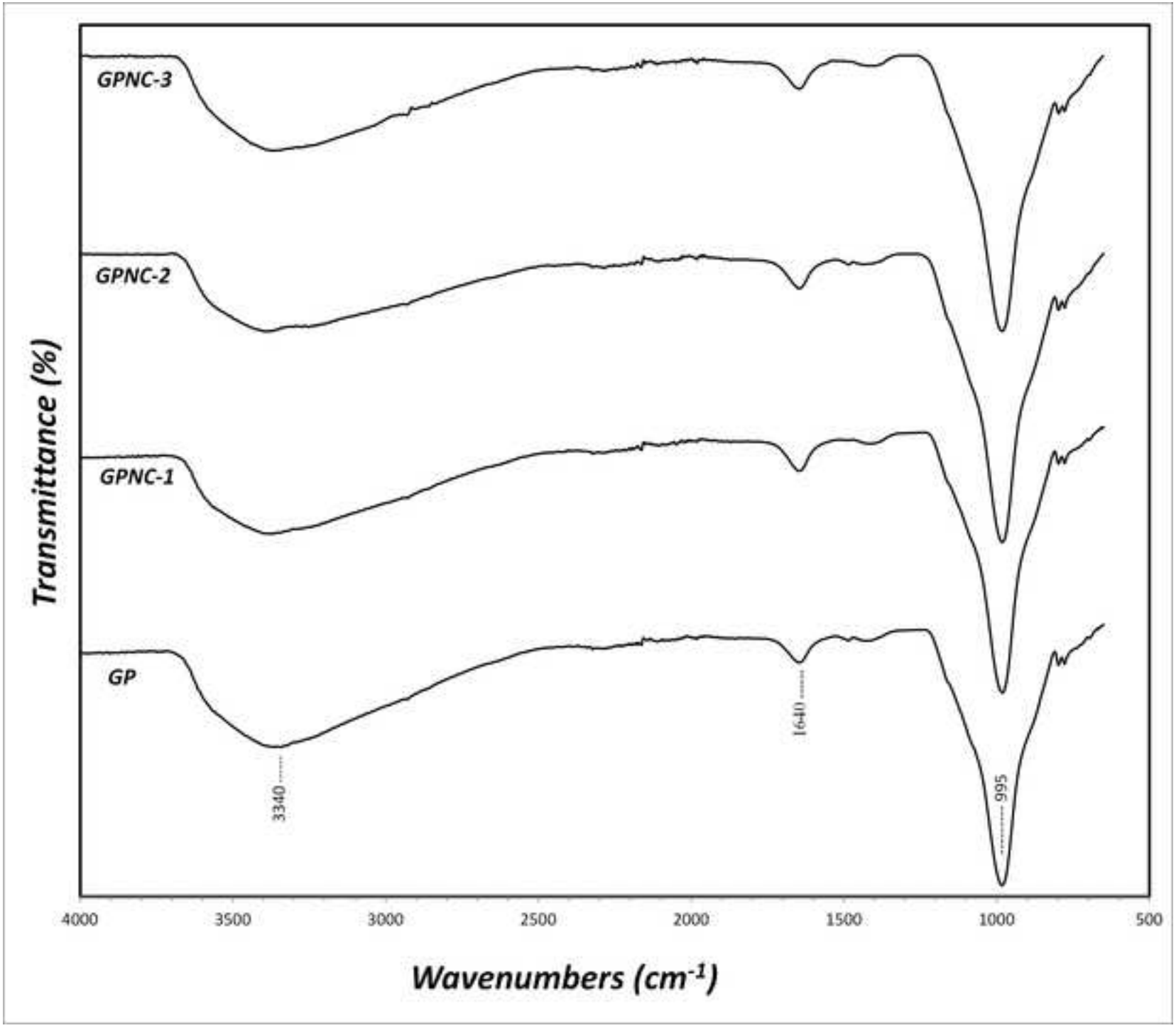

8b_FTIR

Click here to download high resolution image

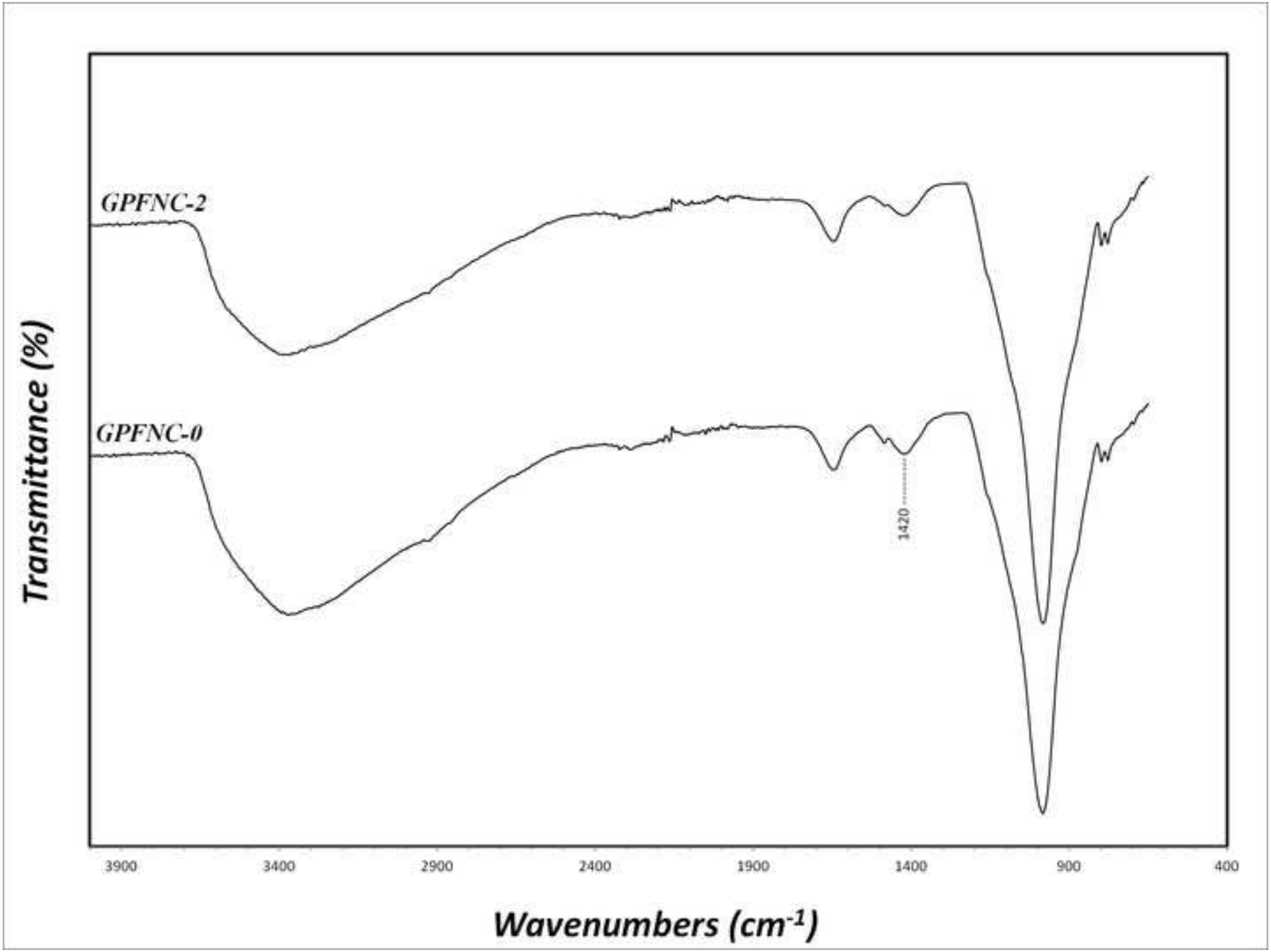

9_FlexuralStrength

Click here to download high resolution image

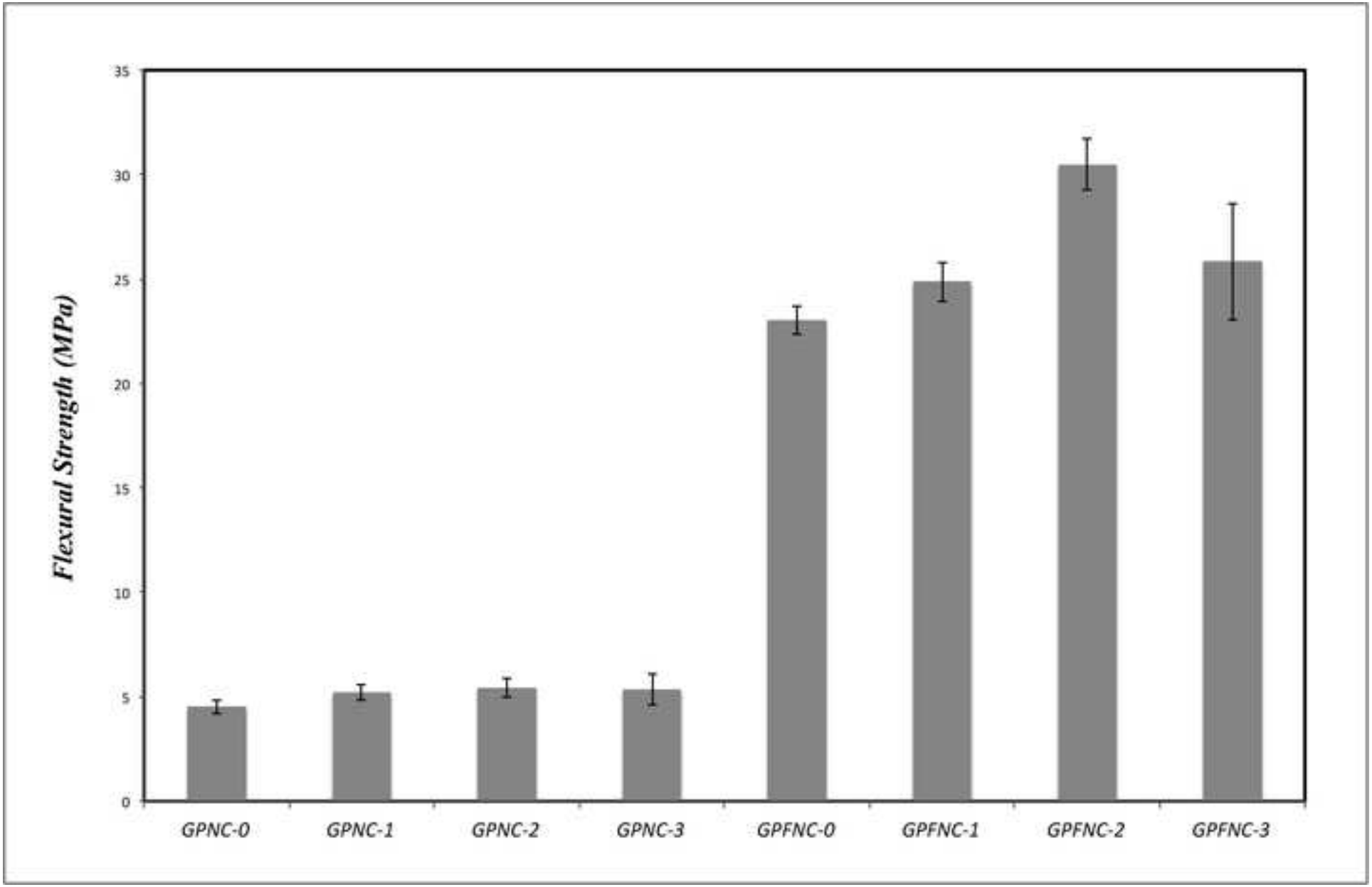

**10a_LoadMidspan**

**Click here to download high resolution image**

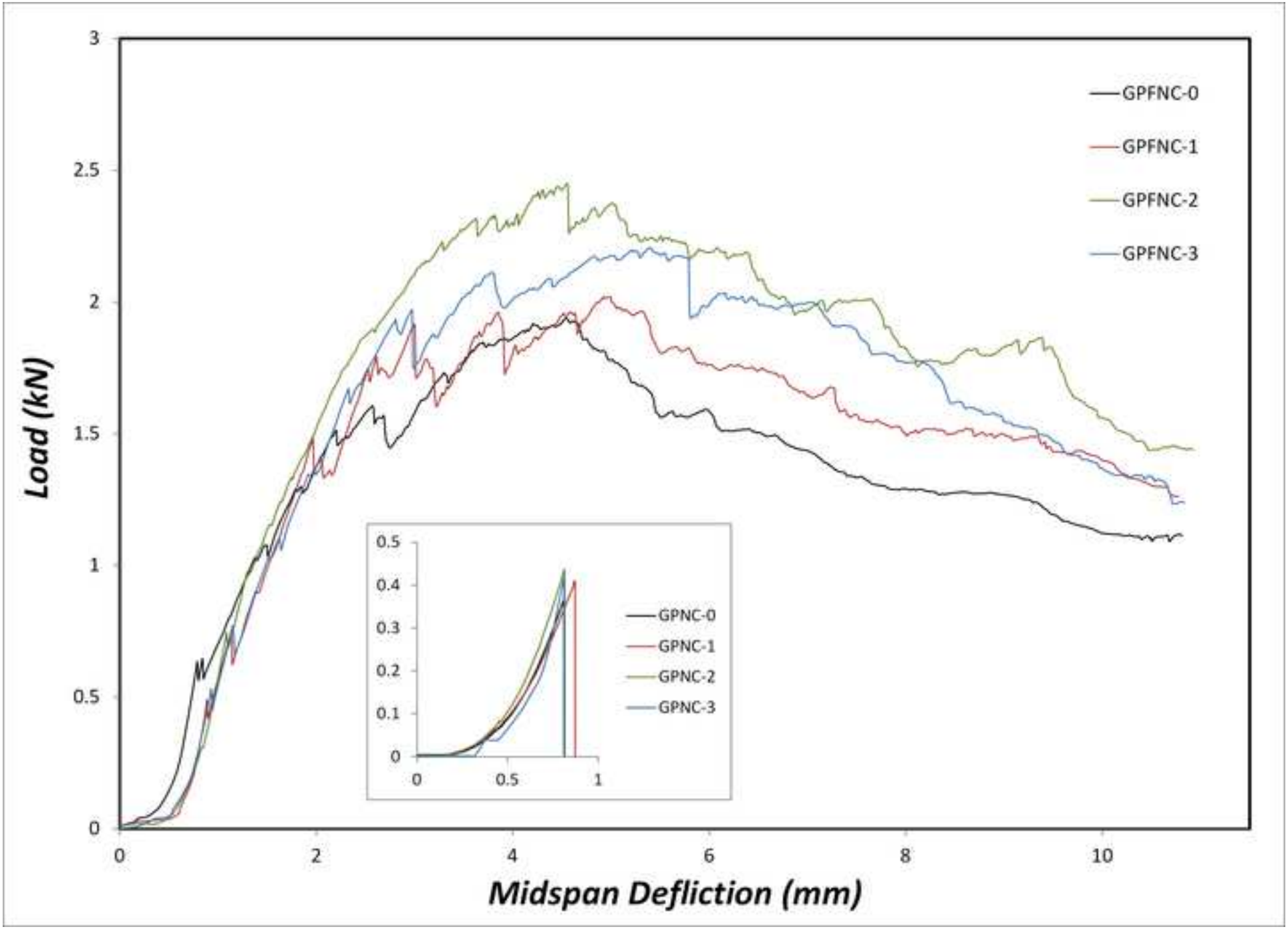

10b_ToughnessIndecis

Click here to download high resolution image

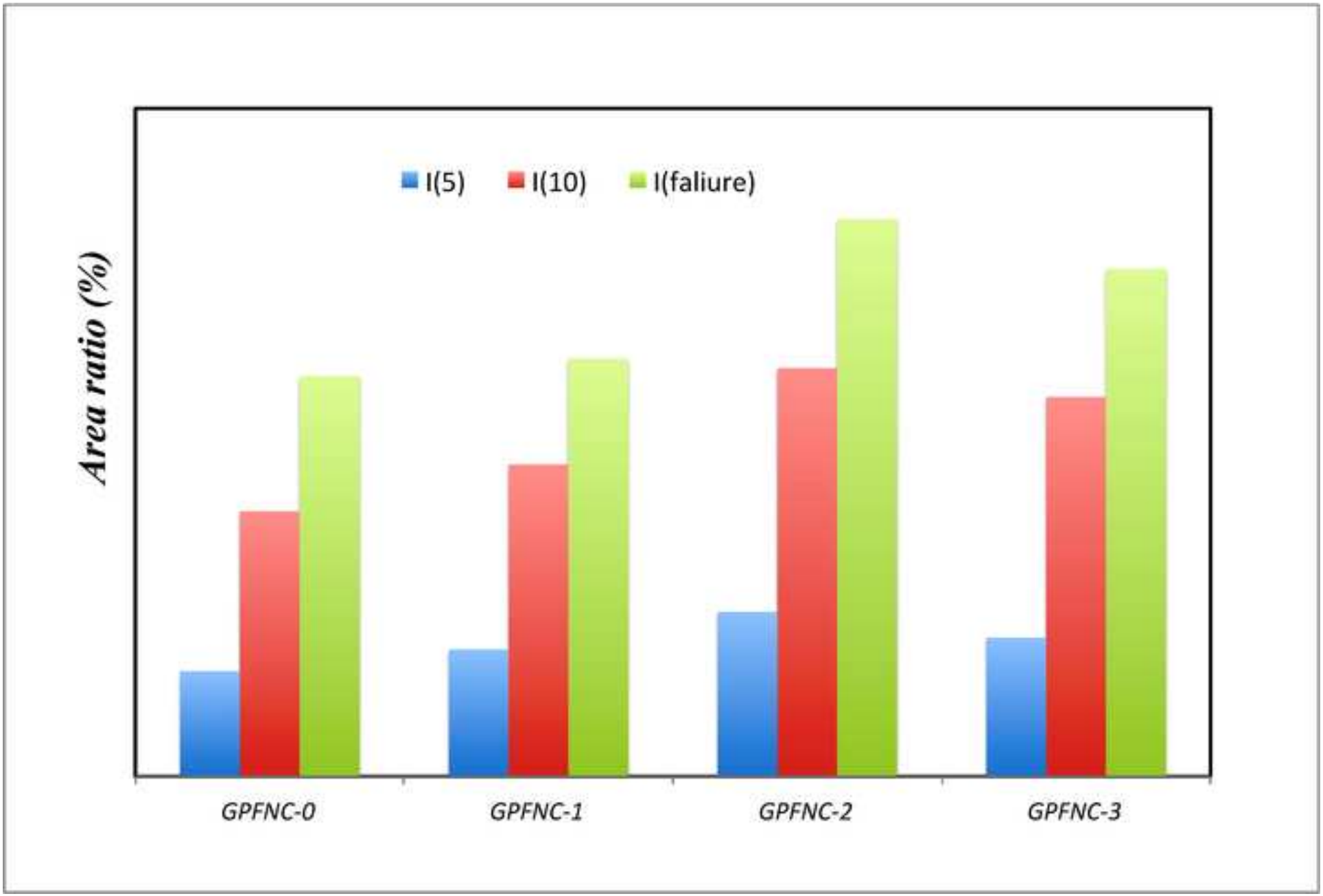

11a_SEM

Click here to download high resolution image

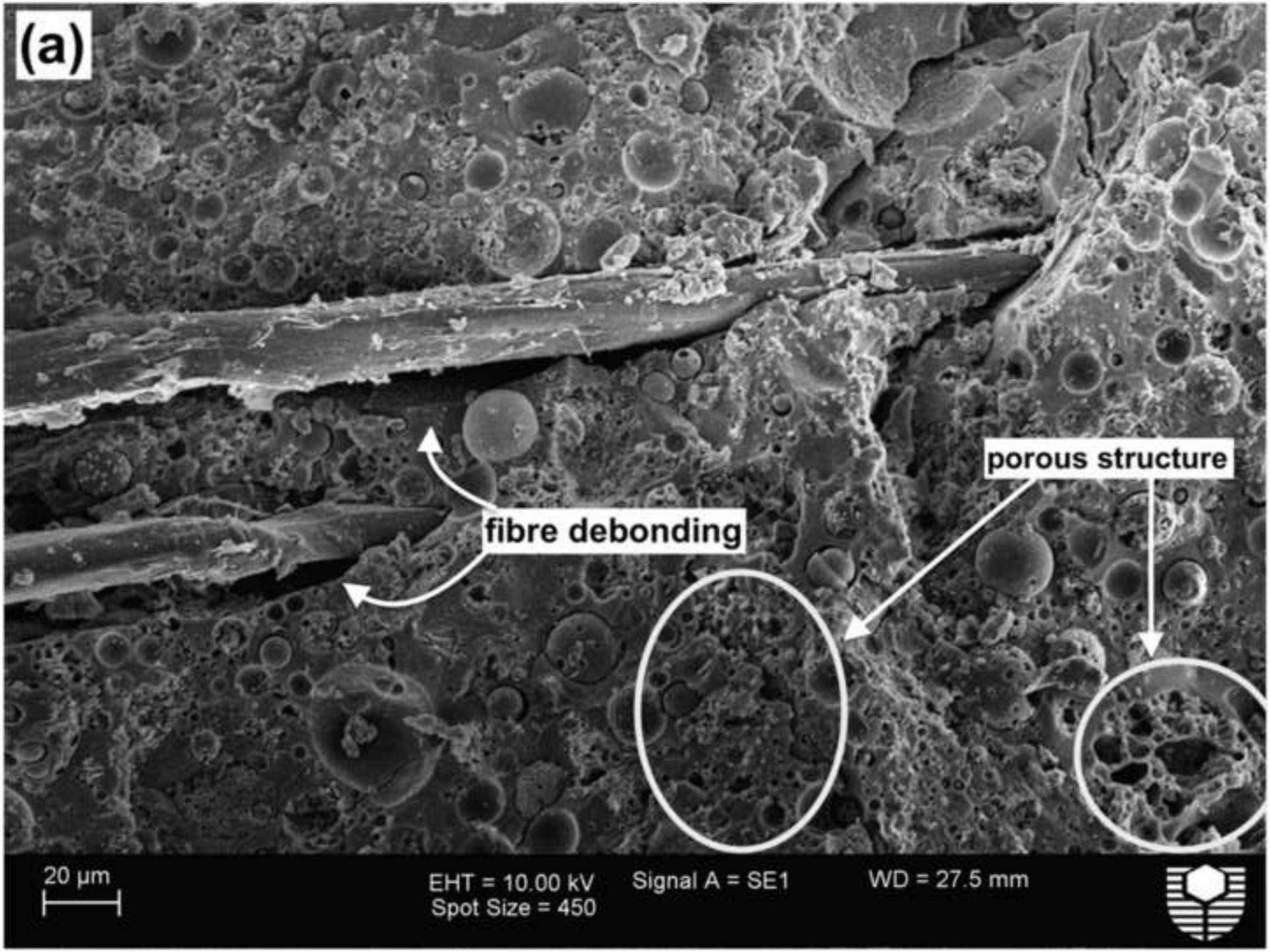

11b_SEM

Click here to download high resolution image

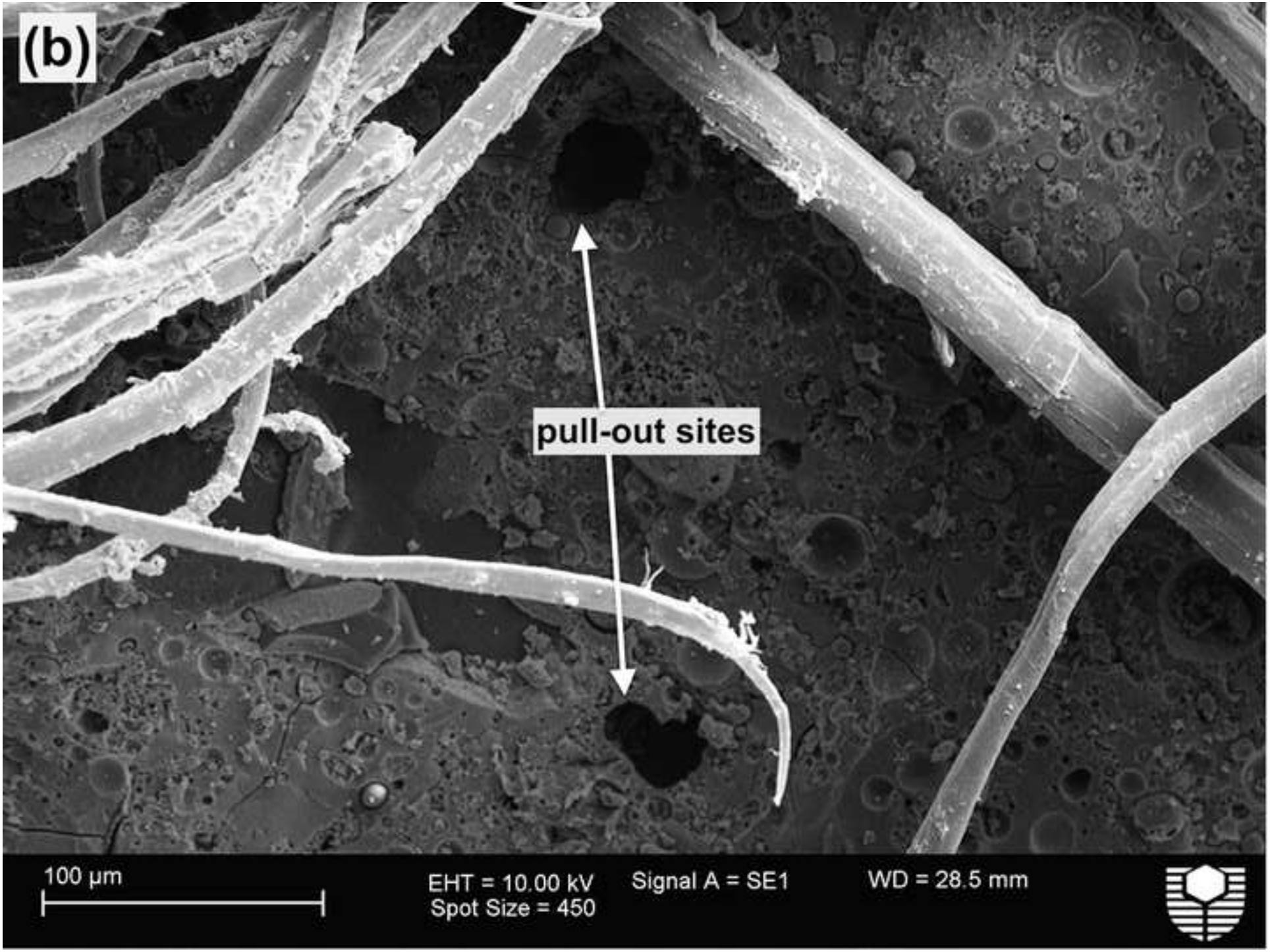

11c_SEM

Click here to download high resolution image

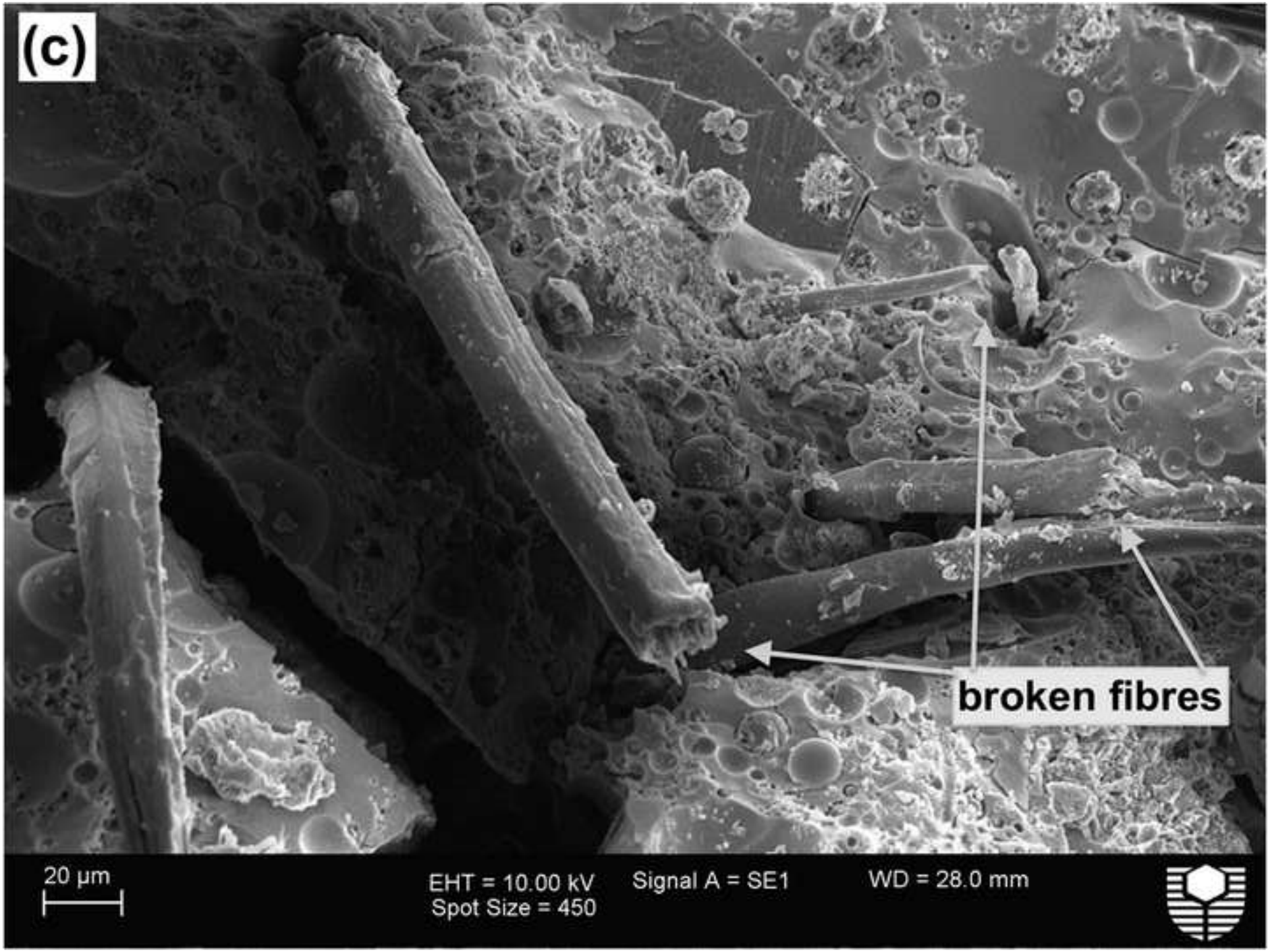

11d_SEM

Click here to download high resolution image